

The microscopic pathway to crystallization in supercooled liquids

John Russo and Hajime Tanaka*

*Institute of Industrial Science, University of Tokyo,
4-6-1 Komaba, Meguro-ku, Tokyo 153-8505, Japan*

Abstract

Despite its fundamental and technological importance, a microscopic understanding of the crystallization process is still elusive. By computer simulations of the hard-sphere model we reveal the mechanism by which thermal fluctuations drive the transition from the supercooled liquid state to the crystal state. In particular we show that fluctuations in bond orientational order trigger the nucleation process, contrary to the common belief that the transition is initiated by density fluctuations. Moreover, the analysis of bond orientational fluctuations shows that these not only act as seeds of the nucleation process, but also i) determine the particular polymorph which is to be nucleated from them and ii) at high density favour the formation of fivefold structures which can frustrate the formation of crystals. These results can shed new light on our understanding of the relationship between crystallization and vitrification.

* e-mail address: tanaka@iis.u-tokyo.ac.jp

The liquid-to-solid transition is characterized by the spontaneous breaking of both positional and orientational symmetry, but how this happens microscopically is still a matter of debate [1–6]. Most approaches, like classical nucleation theory (CNT) or density functional theories (DFT) [7, 8], assume that the crystallization process is primarily controlled by positional ordering, with the liquid regarded as a spatially uniform background where nucleation can occur at any location with an equal probability. However experiments [9–11] and simulations [12–15] have recently started to point out deviations from the classical picture of crystallization, suggesting that this process could be more complex than previously thought.

We argue that for understanding the origin of such deviations it may be crucial to recognize the role of thermally excited fluctuations in driving the transition from the liquid phase to the crystal phase. Fluctuation effects were first identified in globular proteins and colloidal systems close to a metastable critical point, where crystallization starts with the formation of amorphous high-density aggregates and is followed by the actual nucleation event occurring within these fluctuations [16–20]: the *two-step* nucleation scenario. These studies revealed that the coupling between critical concentration fluctuations and density ordering (crystallization) plays a key role in nucleation. Even for a single component liquid, experiments [9–11] and simulations [12, 14] have recently showed the importance of density fluctuations in the initial stage of crystallization, which leads to the formation of precursors. Since the *two-step* nucleation scenario looks valid far [20] or even in absence [14] of a critical point, it has been suggested that this scenario (in which density fluctuations foreshadow structural ordering) could indeed be a general nucleation mechanism. Independently from the aforementioned two-step scenario, recent simulation works [13, 21] have pointed out the importance of another type of fluctuations occurring in the supercooled liquid phase: spontaneous critical-like fluctuations of bond orientational order [22, 23]. While the density order parameter (and in general translational order) is a measure of the relative spacing between the neighbouring particles, bond orientational order expresses instead the relative orientation of the (geometrical) bonds between a particle and its neighbouring particles. In both scenarios, thermal fluctuations promote the formation of crystal precursors, i.e. preordered regions which trigger the nucleation process. However, since density and bond orientational ordering proceed simultaneously in the process of crystal nucleation, it has remained elusive how these order parameters are coupled, and whether any of the two plays a primary role.

In the present work we will investigate precursors in models of colloidal systems in order to elucidate the microscopic mechanism of crystal formation. We use here the word *precursor* as a short term for denoting the region of the liquid’s free energy basin where nucleation is more likely to occur. We will first rule out the possibility of a two-step process involving densification as the first step towards crystallization. We will show instead that the nucleation process proceeds with the crystalline structures emerging first at liquid-like densities, a process akin to what was reported by some studies of nucleation in molecular systems [24, 25]. By examining the crystallization process in the two dimensional order-parameter space of density and orientational order, we will show that precursor regions are not characterized by locally denser regions, but by locally bond-oriented regions, and we will present a novel microscopic explanation of this mechanism. We will show that these precursor regions not only act as seeds of the nucleation process, but also determine the particular polymorph which is to be nucleated from them. This new concept implies that polymorphism is already a property of the metastable liquid state.

It is interesting to note that regions of high bond orientational order have also been identified as responsible for the highly heterogeneous dynamics in deeply supercooled liquids, and could be linked to a growing structural length at the origin of the glass transition [22, 26]. A study of the microscopic properties controlling the crystallization of the liquid is thus of utmost importance not only in elucidating the pathway to crystallization, but potentially also to explain how crystallization can be avoided. In this context, we will show that our two-order parameter description provides a thermodynamic justification of Frank’s hypothesis [27] that icosahedral clusters of particles act as inhibitors of crystallization.

In this Article we concentrate on the homogeneous nucleation process for the simplest nontrivial model of a liquid, hard spheres of diameter σ , by means of computer simulations. This system is ideal for studying crystallization and has already provided tremendous contributions to our basic understanding of crystal nucleation [28–30]. In Supplementary Information we extend the generality of our study by applying the same concepts to very different classes of materials, in particular systems governed by ultrasoft potentials (like polymeric materials) and tetrahedrally coordinated potentials (like water).

Results

Let us start by introducing the order parameters used in this study. We will describe here their basic properties, while for the exact mathematical definition we refer to the Methods section. We will always adopt a microscopic approach, by studying local order parameters (defined at a particle level). Since the liquid-to-solid transition is characterized by both translational and orientational symmetry breaking, we wish to monitor both properties during the crystallization process. A good order parameter for translational order, which expresses the relative spacing between particles in the system, is of course the local density ρ_i . This is easily computed by means of Voronoi diagrams, which assign to each particle a local volume $v_i = 1/\rho_i$. To describe orientational order, which expresses the relative orientation between the neighbours around each particle, we use the spherical harmonics analysis introduced by Steinhardt et al. [31]. We thus define our bond orientational order parameter as $q_6(i)$, which is a rotationally invariant scalar defined for each particle i . A closely related order parameter is $Q_6(i)$, which is obtained by coarse-graining $q_6(i)$ over its neighbours. The importance of Q_6 lies in the fact that it is a good order parameter to detect precursor regions, as we will show later. Finally, to address the question whether crystal nuclei emerge from dense precursors, we need an order parameter that distinguishes disordered configurations from crystal-like ones. We call this order parameter S (as for *structure*): for particle i it goes from a value close to 0 in the liquid-state to a value close to 12 (as the number of neighbours in a close-packed structure) in the crystal state.

Composition of crystals during nucleation and growth

We begin by following 50 spontaneous crystallization events from the metastable state at reduced pressure $\beta p \sigma^3 = 17$, where $\beta = 1/k_B T$ and σ is the hard-spheres diameter. Under these conditions nuclei form and dissolve repeatedly, until the appearance of a nucleus which grows over the critical size and eventually spans the whole system. For each configuration we identify crystal particles following the criteria pioneered by Frenkel and co-workers [28] (see Methods), and identify individual clusters via a cluster algorithm. Figure 1a shows the average number of particles with local bcc, hcp or fcc coordination within the crystal nuclei, as a function of their size. The vertical dashed line in Fig. 1a, which indicates the average

size of the critical nucleus ($n_c \simeq 80$) obtained from umbrella sampling simulations (see Supplementary Information), separates the nucleation and growth regime. Within clusters of size smaller than n_c , $(66 \pm 1)\%$ of the particles are in local fcc coordination. This is markedly different from the ratio for random stacking of hcp and fcc hexagonal planes, $n_{\text{fcc}}/n_{\text{hcp}} \sim 1$, which is predicted from the very small bulk free energy difference (around 0.1% of the thermal energy in favour of fcc) between fcc and hcp phases [32, 33]. This behaviour of hard spheres, also pointed out in earlier studies including both experiments [2, 29, 34–36] and simulations [37–39], remains to our knowledge still unexplained and we will show in the following a mechanism which accounts for this unbalance. The inset of Fig. 1a shows the average density of the crystalline particles as a function of the nucleus size. All crystalline phases form at an average number density of $\sim 1.06\sigma^{-3}$, higher than the metastable liquid density of $\sim 1.02\sigma^{-3}$. The presence of a jump is of course expected for the averaged order parameters (both ρ and q_6) at a first-order phase transition. More surprisingly instead, the density at which the smallest crystals start forming is still very far from the bulk density of the stable crystal ($\rho_s \simeq 1.136\sigma^{-3}$). Thus the nucleation of the solid phase happens under conditions very far from the bulk solid. As the crystal grows, both the densities of the fcc and hcp phases gradually increase, whereas bcc particles are unable to pack efficiently, and hence do not contribute to the cluster growth. Here we note that a bulk bcc crystal is in fact mechanically unstable in hard spheres (meaning that a bulk bcc crystal will immediately transform into a mixture of fcc and hcp crystals).

Now we turn to the order parameter profiles of crystal nuclei. Figure 1b shows the averaged radial profiles of $\rho(r)$ for different sizes of the nucleus (indicated by the arrow). The density profiles gradually increase as the nucleus becomes bigger, but still do not reach the bulk values even for sizes much larger than the critical nucleus size. This is in stark contrast to the prediction of classical nucleation theory (CNT), according to which critical nuclei share the same thermodynamic properties of the bulk solid phase. Such deviations from CNT was predicted by non-classical approaches [24, 40–42]. Contrary to a two-step scenario, where densification foreshadows structuring [14, 20], we find no such an indication, as shown in the inset of Fig. 1b, where the density gap $\Delta\rho$ between the nucleus and the liquid phase is displayed for different radii R/R_{critical} (normalized to the value of the critical radius). The density of the nucleus grows continuously from the liquid, with an almost linear relationship between $\Delta\rho$ and the nucleus size R .

Figure 1c shows both the density radial profile $\rho(r)$ and the profile of the structural order parameter $S(r)$ for critical nuclei ($n \sim 80$). Both profiles are normalized as to be unity in the pure *fcc* crystal, and zero in the bulk liquid phase. Going from the liquid phase ($r = \infty$) to the centre of the nucleus ($r = 0$) we see that the nucleus first develops some structural order at liquid-like densities, and only later does the density increase as well. At the centre of the nucleus both the structural order parameter and the density are far from their bulk values, but density is lagging behind the development of structural order. The inset shows the (S, ρ) -map for nuclei of different sizes. The continuous line is the classical behaviour, while simulation points always fall in the region of structured precursors, and not locally denser precursors. We note that the gradual increase of structural order is rather similar to that reported in [24], where the structural order profile grows both its height and range simultaneously. It may be worth noting that the result in Ref. [24] is derived from a one-order-parameter DFT model, where a perfect decoupling of structural order from density is implicitly assumed. The introduction of a coupling between density and structural order in the same type of model leads instead to the saturation of both structural and density order at the first stages of nucleation [17, 40]. This is an interesting point to be studied since, as described later, our results suggest indeed a weak coupling between the two types of order parameters. In relation to this, we also note that translational order in DFT is not the same as bond orientational order: the former is specific to solid-type fluctuations, but the latter can be linked to both liquid-type and solid-type fluctuations.

In conclusion we have found no signs of the two-step process involving enrichment at constant size and then growth, contrary to some theoretical predictions [14, 20, 42]. We rather find that the density increase is foreshadowed by the prestructuring of the nucleus. This lagging of densification behind structuring is similar to the results of previous nucleation studies in Lennard-Jones systems [8, 17, 25, 40], but with the difference that in these studies both density and structural order are already saturated to the equilibrium values when the nucleus size slightly exceeds the critical size, whereas not in our case (see Fig. 1b and c). Moreover the prestructuring prior to densification has always been ascribed to the low compressibility of the liquid phase (see, e.g., [8]). In the next section we will show instead that density fluctuations in the liquid and crystal phase overlap to a large extent, and that the prestructuring of the nucleus is rather due to the development of orientational order, as the true first step towards crystallization.

Interplay between density and bond orientational order

To explain the nucleation pattern unveiled in the previous section, we will address the question of how density (ρ) and orientational order (q_6) are coupled. In Fig. 2a we display (ρ, q_6) -maps for the metastable liquid (before the appearance of the critical nucleus) at different pressures. We average separately for particles identified as liquid (liquid branch, dashed line) and crystal (crystal branch, lines with symbols) (see also Fig. S1b in Supplementary Information). By comparing the relative position of the two branches in the (ρ, q_6) -map it is easy to spot the regions of stability of each phase: the stable branch lies below the metastable branch, having higher orientational order at fixed density (or conversely, the stable phase can reach the same degree of orientational order at lower packing). Let us start by examining the system at reduced pressure $\beta p \sigma^3 = 11$. This pressure is just below the melting pressure, which is $\beta p \sigma^3 = 11.54$ [43]. As shown in Fig. 2a the liquid branch is always located below the crystal branch, and it is thus the stable branch for all values of q_6 and ρ . This result is of course the expected one, since we are before the melting line. What is surprising is that we are able to determine the relative position of the system with respect to the melting line by simply looking at its (ρ, q_6) map, without resorting to free energy calculations. And again as expected, as we increase the pressure a crossover between the two branches appears, with the crystal branch gaining stability. For clarity we will focus on the curves at $\beta p \sigma^3 = 17$, which is the same pressure at which we obtained our Fig. 1. At low ρ and q_6 the liquid branch is the stable one. The crystal branch remains metastable until it reaches a plateau of constant ρ , where the crossover with the liquid branch occurs. The value of this plateau is $\rho = 1.06\sigma^{-3}$ which is exactly the average density of the onset of crystal formation which we determined in the inset of Fig. 1a. After this plateau the crystal phase thus becomes the stable phase. This means that in the metastable liquid, particles which reach (because of thermal fluctuations) values of q_6 and ρ bigger than the crossover values are in local coordination shells that are transforming from liquid to crystal-like. The reason why this process occurs at constant density is clear if we consider the fact that these particles are already embedded in regions of high orientational order. This means that their neighbours are already highly ordered, and by means of small local rearrangements are able to attain the symmetry of the crystal (in practice crossing the threshold which we use to identify crystal particles). We show an example of such a microscopic process in the snap-

shots in Fig. 2a, where small local rearrangements (white arrows) cause a change of the coordination around the central particle from liquid-like (blue) to crystal-like (red), without changing the local density but by increasing significantly the orientational order.

If we now follow the curve at higher q_6 and ρ a surprising result emerges: a second crossover between the crystal and liquid branches makes the liquid branch stable again. The density of this crossover is $\rho = 1.107\sigma^{-3}$, which corresponds to a volume packing of $\phi \simeq 58\%$ (which is also the conventional value which marks the beginning of the glassy state in hard spheres [30]). This second crossover tells us that at very high q_6 and ρ the crystal phase becomes unfavoured again. Note that these are purely static results, not affected by the underlying dynamics. By using bond orientational analysis (see Supplementary Information), the structures responsible for the stability of the liquid branch at high density are easily identified as particles embedded in icosahedral environments. Icosahedral particles belonging to the liquid branch can attain higher densities than the corresponding crystal structures, but due to their fivefold symmetry are not able to attain long range translational order. The second crossover in the (ρ, q_6) map tells us thus that crystals have a stability window, which is limited at low densities by disordered configurations (larger configurational entropy of liquid particles), and at high density by clusters with icosahedral structure. We have thus shown that icosahedral particles act as inhibitor to crystallization, as was recently observed in both experiments [44, 45] and simulations [46]. This is consistent with a scenario that glass-forming ability is controlled by frustration against crystallization, or the presence of low free-energy local configurations incompatible with the crystal symmetry in a liquid [23, 26, 47–49].

We have seen that the crystallization process is driven by the development of orientational order, which explains the prestructuring of the nuclei at liquid-like densities. Precursor regions are thus easily identified by bond orientational order alone. The one disadvantage of q_6 is that it also reveals the signal from icosahedral environments of particles. To locate crystal precursors, an effective strategy is to spatially coarse-grain q_6 [13, 50], thus enhancing the signal from coherent regions (crystal-like) and suppressing it in disordered or icosahedral-like regions. This is the order parameter called Q_6 , which grows continuously from the liquid branch to the crystal branch. In Fig. 2b we plot, for the metastable liquid (prior to the appearance of the critical nuclei) at pressure $\beta p\sigma^3 = 17$, a map in the (Q_6, ρ) plane of the structural order parameter S . $S(i)$ quantifies how many first-shell neighbours of particle i

have similar local environments: for a disordered liquid we expect S to be null, whereas for a bulk close-packed crystal to be 12, i.e. all neighbours share the same environment. As we can see from Fig. 2b the structural order parameter grows ‘continuously’ from low Q_6 to high Q_6 values. Contour lines are almost parallel to the ρ axis, meaning that density is only weakly coupled to the increase of crystalline structure. In other words, high density regions encompass all possible values of the S , while high Q_6 regions are always the most crystalline. So precursor regions are exclusively controlled by the coarse-grained orientational order parameter, and density fluctuations are not sufficient to promote crystallization.

Polymorph selection

Crystals repeatedly appear, grow and melt as represented by the fluctuations in the bond orientational order parameter Q_6 . Since crystal nuclei appear from regions of high bond orientational order, the study of such regions should provide important information on the forming nuclei. In particular we will show that not only the precursor regions act as seed for crystal growth, but they also determine which polymorph will be nucleated from them. To do so we use the order parameters W_4 and W_6 , which are very useful in the detection of polymorphs. We report their exact definition in the Methods section, and just report here their basic properties. W_6 is a good order parameter to distinguish between bcc crystals and close-packed crystals (hcp and/or fcc), since it is positive in the former whereas negative for the latter. W_4 is instead good to distinguish between fcc crystals (for which it has negative values) and hcp crystals (for which it has positive values). Figure 3a shows the probability distribution for the order parameter W_4 in liquid regions having Q_6 higher than a fixed threshold, Q_6^{thr} . The W_4 distribution was obtained by considering only liquid particles (crystal particles are not included in the histogram) in the metastable state (before the critical nucleus is formed), and the Q_6^{thr} threshold values are always within the liquid distribution. While the metastable liquid has on average a symmetrical distribution around $W_4 = 0$, Fig. 3a reveals that the high Q_6 regions have a predominant contribution from negative values of W_4 , which correspond to the fcc symmetry. Similar histograms are obtained if instead of thresholds one uses small Q_6 intervals centered at progressively high values of Q_6 (always within the liquid distribution).

Since we have shown that crystals form from particles of high Q_6 , the following scenario

emerges for the nucleation of hard-sphere crystals: the supercooled liquid develops regions of high orientational order (Fig. 2b), whose symmetry favours the nucleation of the fcc phase (Fig. 3a). Figure 3b plots the probability distribution for the order parameter W_6 , showing that indeed the regions of high Q_6 display no preference for the bcc symmetry (characterized by $W_6 > 0$). Figure 3c displays the radial distribution function, $g(r)$, for the same high Q_6 regions. Notably, higher Q_6 regions show an enhancement of the shoulder in the second peak of the pair distribution function, which is known to be a structural precursor to the freezing transition [51]. The fact that regions of high Q_6 are more prone to crystallization can also be seen in Fig. 3d, where the two-body excess entropy [52, 53], s_2 , is plotted for different values of the threshold Q_6^{thr} . It is known that the two-body excess entropy forms the dominant contribution to the excess entropy, of the order of 85 – 90% in simple monoatomic liquids. Its value is $s_2 = -6.8$ for the metastable liquid, and $s_2 \cong -10$ for the bulk crystal. The inset shows that the s_2 value indeed rapidly decreases for increasing values of the threshold Q_6^{thr} . Moreover, the dashed and dotted-dashed lines display the values of s_2 calculated for particles having $W_4 < 0$ (fcc-like) and $W_4 > 0$ (hcp-like) respectively, demonstrating that there is a large difference in the configurational entropy (at the two-particle level) between particles having fcc and hcp symmetry, the former ones being strongly favoured towards crystallization (the difference between the s_2 value of hcp and fcc-like particles is of the order of 1%). This implies that although fcc and hcp have the same free energy in bulk, small clusters of fcc symmetry have a lower free energy (lower configurational, but higher correlational entropy) than those of hcp symmetry.

Discussions

In this Article we have studied the process of crystallization from the perspective of both local translational and bond orientational order. Crystallization has so far been described by translational ordering of the density field. However, our study clearly indicates that symmetry selection due to packing constraint or directional bonding (like in water, see Supplementary Information), which is represented by bond orientational order, plays a key role in the crystallization process. It is bond orientational order and neither density nor translational order that triggers crystal nucleation. Structuring before densification was also reported in Refs. [18, 25, 54] for molecular liquids, in which the range of the interaction

is longer than the size of the constitutive particles. For these liquids, the DFT approach showed that the density of the critical nucleus might deviate significantly from the bulk phases, and that the compactification of the nuclei has to be accompanied by an increase of their local structure (i.e. lattice periodicity). This nucleation mechanism is often ascribed to the low compressibility of the liquid, which favours structuring prior to densification upon nucleation [8]. Contrary to this scenario, our results suggest that this behaviour is a consequence of the weak coupling between density fluctuations and bond-order fluctuations, with the latter driving the crystallization process. In other words, it is due to the fact that nuclei form in precursors of high orientational order, where small displacements can considerably increase the order with very little density change (see the pictures in Fig. 2a). The increase in the structural order parameter is thus inherited from a well defined region of the metastable liquid phase space, characterized by having high orientational order. Note that high density regions are not necessarily characterized by high orientational order, and thus they alone cannot trigger the nucleation process. The existence of these regions of high density and low orientational order suggests that it is not the low compressibility of the liquid which is responsible for the coupling between density and orientational order.

Moreover we found that regions of high bond orientational order within the metastable liquid not only act as crystal precursors but can also determine which particular crystal polymorph will nucleate from them, even when precritical nuclei (which naturally populate the metastable phase) are disregarded from the analysis. Since the large population of sub-critical embryos belongs to the same metastable free energy basin of the liquid (as can be seen for example in Fig. 2b), it is natural to expect that the emergence of polymorphism will be a continuous process starting in the liquid phase. Polymorphism develops together with bond orientational order, highlighting the role of precursor regions in the polymorph selection process. A liquid has orientationally ordered precursor regions which can exist in a variety of crystal symmetries, according to some high-dimensional probability distribution. For hard spheres, the projections of this probability distribution along some reaction coordinates are reported in Fig. 3, and show that precursor regions with the fcc-symmetry are more abundant than hcp-symmetry regions. So if a nucleation event occurs in any of these regions, the crystal environment will reflect the symmetry of the precursor, or the symmetry favoured in a liquid. For hard spheres, the preference towards fcc was pointed out in earlier studies, both experiments [2, 29, 34–36] and simulations [37–39], and can be explained classically neither

by Ostwald’s step rule nor by the Alexander-McTague scenario [55]. While correctly pointing to the relevance of metastable states, Ostwald’s rule cannot be literally applied to predict the outcome of a nucleation process. Instead, we have shown that the relative abundance of one polymorph over the other depends directly on the liquid-state precursor’s composition. This may be related to the scenario proposed by Stranski and Totomanow [56], where the embryos that form most readily are those with the lowest free energy barrier to nucleation. Our results suggest that the physical mechanism behind this rule is a matching of bond orientational symmetry between precursor regions and crystals, which leads to the reduction of the free barrier for nucleation (the interfacial energy). To give a more quantitative account of this scenario, we also calculated the pair correlation entropy of precursor regions (Fig. 3), showing indeed an imbalance between the different crystal symmetries. We confirm that this scenario of crystallization and the resulting selection mechanism of polymorphs are also valid for soft spheres (the Gaussian Core model) [57] and water (see Supplementary Information). These results could help clarifying the mechanism behind the interplay between crystallization and liquid polymorphism which was recently found for both water [58] and silicon [59].

Our two-dimensional analysis also unveiled a density range of stability of the crystals which continuously form in the metastable liquid. This range of stability is limited at low densities by the usual disordered liquid configurations, and at high densities by fivefold arrangements of particles. This result, obtained from purely static arguments, provides a thermodynamic justification of Frank’s hypothesis [27] that icosahedral clusters of particles act as inhibitors of crystallization. This finding may enhance our understanding of the nature of a supercooled metastable liquid state and crystallization, possibly shedding light on the interplay between crystallization and vitrification [60]. Liquid and crystal often have very different densities, due to the translational order of the latter. However, our study reveals that bond orientational order is the first step in the pathway from the liquid to the crystal state, and a disconnection of this link by competing orientational orderings or random disorder may be responsible for the avoidance of crystallization, i.e. vitrification (see Fig. 2a and Refs. [23, 26]).

Methods

We study the crystallization process in a system of $N = 4000$ monodisperse hard spheres of diameter σ by means of isothermal-isobaric (NPT) Monte Carlo simulations. Lengths are given in units of the particle diameter σ and pressure in units of $k_B T / \sigma^3$, where $k_B T = 1$. We place the spheres randomly in a simulation box at packing fraction $\eta = 0.5352$ and equilibrate the system at reduced pressure $\beta p \sigma^3 = 17.0$. At this pressure the liquid is metastable with respect to crystallization, with a difference in chemical potential between the liquid and solid state of $\beta |\Delta\mu| = 0.54$. As shown in [39] the free energy barrier between the metastable liquid phase and the crystal phase is $\beta \Delta F \simeq 18$, and the size of the critical nucleus is $\simeq 80$. Under this conditions crystallization is a rare event, for which not only long trajectories can be obtained for the supercooled liquid, but also enough nucleation events can be observed spontaneously.

To identify crystal particles we use the local bond-order analysis introduced by Steinhardt et al. [31]. One first introduces a $(2l + 1)$ dimensional complex vector (\mathbf{q}_l) , which is defined for each particle i as $q_{lm}(i) = \frac{1}{N_b(i)} \sum_{j=1}^{N_b(i)} Y_{lm}(\hat{\mathbf{r}}_{ij})$, where l is a free integer parameter, m is an integer that runs from $m = -l$ to $m = l$, Y_{lm} are the spherical harmonics, $\hat{\mathbf{r}}_{ij}$ is the vector from particle i to particle j , and the sum goes over all neighbouring particles $N_b(i)$ of particle i . Since for hard spheres it is known that the stable crystals are the close packed structures we can impose $N_b(i) = 12$, i.e. we consider only the 12 nearest neighbours (a procedure which is density independent and greatly improves the statistics). From the vectors \mathbf{q}_l one can construct different invariants, and our bond orientational order parameter is one of them, specifically $q_6(i) = \sqrt{4\pi \sum_{m=-6}^6 |q_{6m}(i)|^2 / (2l + 1)}$. The vectors \mathbf{q}_l have been proven to be useful also to identify crystal particles within the liquid. This procedure, first applied to study nucleation by Frenkel and co-workers [28], consists of comparing the orientational environments of two neighbouring particles via a scalar product $\mathbf{q}_6(i)/|\mathbf{q}_6(i)| \cdot \mathbf{q}_6(j)/|\mathbf{q}_6(j)|$. If the scalar product between two neighbours exceeds 0.7 then the two particles are deemed *connected*. We then identify particle i as being within a *crystal* if it is connected with at least 7 neighbours, and otherwise within a *liquid*. The structural order parameter, $S(i)$, of a particle i (which we employed in Fig. 1c and Fig. 2b) simply expresses the number of connected neighbours in a continuous way, i.e. $S_i = \sum_{j=1}^{N_b(i)} \frac{\mathbf{q}_6(i) \cdot \mathbf{q}_6(j)}{|\mathbf{q}_6(i)| |\mathbf{q}_6(j)|}$.

To distinguish between the different crystal polymorphs we employ the spatially aver-

aged local bond order parameters introduced in Ref. [50]. We first define the quantities $\hat{q}_{lm}(i) = \frac{1}{N_b(i)} \sum_{k=0}^{N_b(i)} q_{lm}(k)$. Given the previous definition, one can construct the rotationally invariant quantities

$$Q_l(i) = \sqrt{4\pi/(2l+1)} |\hat{\mathbf{q}}_l(i)|$$

and

$$W_l(i) = \sum_{m_1, m_2, m_3=0}^l \begin{pmatrix} l & l & l \\ m_1 & m_2 & m_3 \end{pmatrix} \frac{\hat{q}_{lm_1}(i) \hat{q}_{lm_2}(i) \hat{q}_{lm_3}(i)}{|\hat{\mathbf{q}}_l(i)|^3}$$

where the term in parentheses is the Wigner 3-j symbol (which is different from zero only when $m_1 + m_2 + m_3 = 0$).

More details about these analyses are given in Supplementary Information.

-
- [1] Kelton, K. F. & Greer, A. L. *Nucleation in Condensed Matter: Applications in Materials and Biology* (Pergamon, 2010).
 - [2] Palberg, T. Colloidal crystallization dynamics. *Curr. Opin. Colloid Interface Sci.* **2**, 607–614 (1997).
 - [3] Anderson, V. J. & Lekkerkerker, H. N. W. Insights into phase transition kinetics from colloid science. *Nature* **416**, 811–815 (2002).
 - [4] Auer, S. & Frenkel, D. Numerical simulation of crystal nucleation in colloids. *Adv. Polym. Sci.* **173**, 149–207 (2005).
 - [5] Sear, R. Nucleation: Theory and applications to protein solutions and colloidal suspensions. *J. Phys.: Condens. Matter* **19**, 033101 (2007).
 - [6] Gasser, U. Crystallization in three- and two-dimensional colloidal suspensions. *J. Phys.: Condens. Matter* **21**, 203101 (2009).
 - [7] Baus, M. Statistical mechanical theories of freezing: An overview. *J. Stat. Phys.* **48**, 1129–1146 (1987).
 - [8] Oxtoby, D. W. Nucleation of first-order phase transitions. *Acc. Chem. Res.* **31**, 91–97 (1998).
 - [9] Schöpe, H. J., Bryant, G. & van Meegen, W. Two-step crystallization kinetics in colloidal hard-sphere systems. *Phys. Rev. Lett.* **96**, 175701 (2006).

- [10] Savage, J. R. & Dinsmore, A. D. Experimental evidence for two-step nucleation in colloidal crystallization. *Phys. Rev. Lett.* **102**, 198302 (2009).
- [11] Iacopini, S., Palberg, T. & Schöpe, H. J. Crystallization kinetics of polydisperse hard-sphere-like microgel colloids: Ripening dominated crystal growth above melting. *J. Chem. Phys.* **130**, 084502 (2009).
- [12] O'Malley, B. & Snook, I. Structure of hard-sphere fluid and precursor structures to crystallization. *J. Chem. Phys.* **123**, 054511 (2005).
- [13] Kawasaki, T. & Tanaka, H. Formation of a crystal nucleus from liquid. *Proc. Nat. Acad. Sci. U.S.A.* **107**, 14036 (2010).
- [14] Schilling, T., Schöpe, H. J., Oettel, M., Opletal, G. & Snook, I. Precursor-mediated crystallization process in suspensions of hard spheres. *Phys. Rev. Lett.* **105**, 25701 (2010).
- [15] Lechner, W., Dellago, C. & Bolhuis, P. G. Role of the prestructured surface cloud in crystal nucleation. *Phys. Rev. Lett.* **106**, 85701 (2011).
- [16] ten Wolde, P. R. & Frenkel, D. Enhancement of protein crystal nucleation by critical density fluctuations. *Science* **277**, 1975–1978 (1997).
- [17] Shen, Y. C. & Oxtoby, D. W. Nucleation of Lennard-Jones fluids: A density functional approach. *J. Chem. Phys.* **105**, 6517–6524 (1996).
- [18] Oxtoby, D. W. Crystal nucleation in simple and complex fluids. *Philos. T. Roy. Soc. A* **361**, 419–428 (2003).
- [19] Lutsko, J. F. A dynamical theory of nucleation for colloids and macromolecules. *J. Chem. Phys.* **136**, 034509 (2012).
- [20] Lutsko, J. F. & Nicolis, G. Theoretical evidence for a dense fluid precursor to crystallization. *Phys. Rev. Lett.* **96**, 46102 (2006).
- [21] Kawasaki, T. & Tanaka, H. Structural origin of dynamic heterogeneity in three-dimensional colloidal glass formers and its link to crystal nucleation. *J. Phys.: Condens. Matter* **22**, 232102 (2010).
- [22] Tanaka, H., Kawasaki, T., Shintani, H. & Watanabe, K. Critical-like behaviour of glass-forming liquids. *Nature Mater.* **9**, 324–331 (2010).
- [23] Tanaka, H. Bond orientational ordering in a metastable supercooled liquid: a shadow of crystallization and liquid-liquid transition. *J. Stat. Mech.* **2010**, P12001 (2010).
- [24] Bagdassarian, C. K. & Oxtoby, D. W. Crystal nucleation and growth from the undercooled

- liquid: A nonclassical piecewise parabolic free-energy model. *J. Chem. Phys.* **100**, 2139 (1994).
- [25] ten Wolde, P. R., Ruiz-Montero, M. J. & Frenkel, D. Numerical calculation of the rate of crystal nucleation in a Lennard-Jones system at moderate undercooling. *J. Chem. Phys.* **104**, 9932 (1996).
 - [26] Shintani, H. & Tanaka, H. Frustration on the way to crystallization in glass. *Nature Phys.* **2**, 200–206 (2006).
 - [27] Frank, F. C. Supercooling of liquids. *P. Roy. Soc. Lond. A Mat.* **215**, 43–46 (1952).
 - [28] Auer, S. & Frenkel, D. Numerical prediction of absolute crystallization rates in hard-sphere colloids. *J. Chem. Phys.* **120**, 3015–3029 (2004).
 - [29] Gasser, U., Weeks, E. R., Schofield, A., Pusey, P. N. & Weitz, D. A. Real-space imaging of nucleation and growth in colloidal crystallization. *Science* **292**, 258 (2001).
 - [30] Zaccarelli, E. *et al.* Crystallization of hard-sphere glasses. *Phys. Rev. Lett.* **103**, 135704 (2009).
 - [31] Steinhardt, P. J., Nelson, D. R. & Ronchetti, M. Bond-orientational order in liquids and glasses. *Phys. Rev. B* **28**, 784–805 (1983).
 - [32] Bolhuis, P. G., Frenkel, D., Mau, S. C. & Huse, D. A. Entropy difference between crystal phases. *Nature* **388**, 235–236 (1997).
 - [33] Pronk, S. & Frenkel, D. Can stacking faults in hard-sphere crystals anneal out spontaneously? *J. Chem. Phys.* **110**, 4589–4592 (1999).
 - [34] Pusey, P. N. *et al.* Structure of crystals of hard colloidal spheres. *Phys. Rev. Lett.* **63**, 2753–2756 (1989).
 - [35] Dux, C. & Versmold, H. Light diffraction from shear ordered colloidal dispersions. *Phys. Rev. Lett.* **78**, 1811–1814 (1997).
 - [36] Cheng, Z., Zhu, J., Russel, W. B., Meyer, W. V. & Chaikin, P. M. Colloidal hard-sphere crystallization kinetics in microgravity and normal gravity. *Appl. Optics* **40**, 4146–4151 (2001).
 - [37] Luchnikov, V., Gervois, A., Richard, P., Oger, L. & Troadec, J. P. Crystallization of dense hard sphere packings Competition of hcp and fcc close order. *J. Mol. Liq.* **96**, 185–194 (2002).
 - [38] O’Malley, B. & Snook, I. Crystal nucleation in the hard sphere system. *Phys. Rev. Lett.* **90**, 85702 (2003).
 - [39] Fillion, L., Hermes, M., Ni, R. & Dijkstra, M. Crystal nucleation of hard spheres using molecular dynamics, umbrella sampling, and forward flux sampling: A comparison of simulation techniques. *J. Chem. Phys.* **133**, 244115 (2010).

- [40] Harrowell, P. & Oxtoby, D. W. A molecular theory of crystal nucleation from the melt. *J. Chem. Phys.* **80**, 1639–1646 (1984).
- [41] Baidakov, V., Boltashev, G. & Schmelzer, J. Comparison of different approaches to the determination of the work of critical cluster formation. *J. Colloid Interf. Sci.* **231**, 312–321 (2000).
- [42] Philippe, T. & Blavette, D. Minimum free-energy pathway of nucleation. *J. Chem. Phys.* **135**, 134508 (2011).
- [43] Noya, E. G., Vega, C. & de Miguel, E. Determination of the melting point of hard spheres from direct coexistence simulation methods. *J. Chem. Phys.* **128**, 154507 (2008).
- [44] Kelton, K. F. *et al.* First X-ray scattering studies on electrostatically levitated metallic liquids: demonstrated influence of local icosahedral order on the nucleation barrier. *Phys. Rev. Lett.* **90**, 195504 (2003).
- [45] Royall, C. P., Williams, S. R., Ohtsuka, T. & Tanaka, H. Direct observation of a local structural mechanism for dynamic arrest. *Nature Mater.* **7**, 556–561 (2008).
- [46] Karayiannis, N. C., Malshe, R., de Pablo, J. J. & Laso, M. Fivefold symmetry as an inhibitor to hard-sphere crystallization. *Phys. Rev. E* **83**, 061505 (2011).
- [47] Tanaka, H. A simple physical model of liquid-glass transition: Intrinsic fluctuating interactions and random fields hidden in glass-forming liquids. *J. Phys.: Condens. Matter* **10**, L207–L214 (1998).
- [48] Taffs, J., Malins, A., Williams, S. & Royall, C. The effect of attractions on the local structure of liquids and colloidal fluids. *J. Chem. Phys.* **133**, 244901 (2010).
- [49] Leocmach, M. & Tanaka, H. Roles of icosahedral and crystal-like order in hard spheres glass transition *Nat. Commun.* in print (2012).
- [50] Lechner, W. & Dellago, C. Accurate determination of crystal structures based on averaged local bond order parameters. *J. Chem. Phys.* **129**, 114707 (2008).
- [51] Truskett, T. M., Torquato, S., Sastry, S., Debenedetti, P. G. & Stillinger, F. H. Structural precursor to freezing in the hard-disk and hard-sphere systems. *Phys. Rev. E* **58**, 3083 (1998).
- [52] Baranyai, A. & Evans, D. J. Direct entropy calculation from computer simulation of liquids. *Phys. Rev. A* **40**, 3817 (1989).
- [53] Truskett, T. M., Torquato, S. & Debenedetti, P. G. Towards a quantification of disorder in materials: Distinguishing equilibrium and glassy sphere packings. *Phys. Rev. E* **62**, 993

- (2000).
- [54] Oettel, M. Mode expansion for the density profile of crystal-fluid interfaces: Hard spheres as a test case. *arXiv:1203.3756* (2012).
 - [55] Alexander, S. & McTague, J. Should all crystals be bcc? Landau theory of solidification and crystal nucleation. *Phys. Rev. Lett.* **41**, 702–705 (1978).
 - [56] Stranski, N. I. & Totomanow, D. Rate of formation of (crystal) nuclei and the Ostwald step rule. *Z. Phys. Chem.* **163**, 399–408 (1933).
 - [57] Russo, J. & Tanaka, H. Selection mechanism of polymorphs in the crystal nucleation of the Gaussian core model. *Soft Matter* **8**, 4206–4215 (2012).
 - [58] More, E. B. & Molinero, V. Structural transformation in supercooled water controls the crystallization rate of ice. *arXiv:1107.1622v1* (2011).
 - [59] Desgranges, C. & Delhommelle, J. Role of liquid polymorphism during the crystallization of Silicon. *J. Am. Chem. Soc.* (2011).
 - [60] Sanz, E. *et al.* Crystallization mechanism of hard sphere glasses. *Phys. Rev. Lett.* **106**, 215701 (2011).

Acknowledgments The authors thank Mathieu Leocmach, Flavio Romano and Laura Filion for fruitful discussions. We thank Marjolein Dijkstra, Daan Frenkel and Francesco Sciortino for a critical reading of an earlier version of the manuscript. This work was partially supported by a grant-in-aid from the Ministry of Education, Culture, Sports, Science and Technology, Japan and Aihara Project, the FIRST program from JSPS, initiated by CSTP.

Author Contributions H. T. conceived the research, J. R. performed simulations, J. R. and H. T. discussed and wrote the manuscript.

Additional Information The authors declare that they have no competing financial interests. Correspondence and requests for materials should be addressed to H. T.

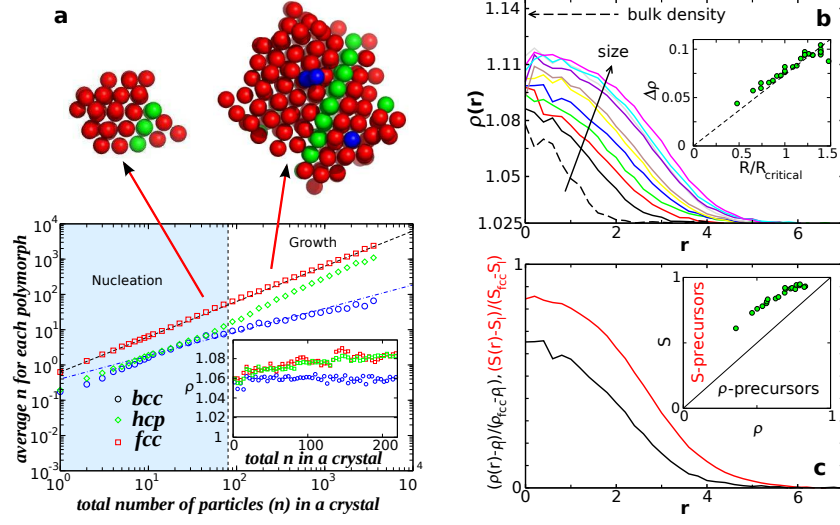


FIG. 1: **Composition and radial profiles for crystalline nuclei averaged over many independent trajectories at $\beta p \sigma^3 = 17$.** **a**, Relation between cluster size and polymorphs. Average number of particles for bcc (circles), hcp (diamonds) and fcc (squares) polymorphs as a function of the total crystal size (n). The dashed line grows as the volume, $\sim n$, whereas the dashed-dotted line grows as the surface, $\sim n^{2/3}$. The vertical dashed line indicates the critical nucleus size n_c , which separates the nucleation regime (the tint blue colour region) and the growth regime. The inset shows the average density of particles belonging to the different polymorphs, and the continuous line the average density of the liquid phase. Also shown are two examples of snapshots of crystal nuclei from the computer simulations, at sizes $n = 40$ (left) and $n = 220$ (right). The particles are coloured according to the following code: fcc (red), hcp (green), and bcc (blue). **b**, Average density profiles as a function of the distance r from the centre of mass of the nucleus. Lines are density profiles for nuclei of sizes between $n = 5$ and $n = 205$ (plotted every $\Delta n = 20$ with the order given by the arrow); each density profile is averaged over nuclei of sizes $n \pm 5$. Crystals are nucleated at conditions very far from the bulk value, indicated by the dashed horizontal line. The inset shows the density difference $\Delta\rho$ between the centre of the nucleus and the liquid density, as a function of the normalized nucleus size (R/R_{critical}). **c**, Comparison between the density profile ($\rho(r)$ black line) and the structural order parameter profile ($S(r)$ red line) for the critical nucleus (size $n = 80$). Both profiles are normalized to be unity in the *fcc* crystal state, and zero in the liquid phase. The inset shows the (S, ρ) -map for nuclei of different sizes (the same as in the panel *b*). The continuous line is the classical behaviour, while simulation results show that nuclei form in ordered precursors, and not locally denser precursors.

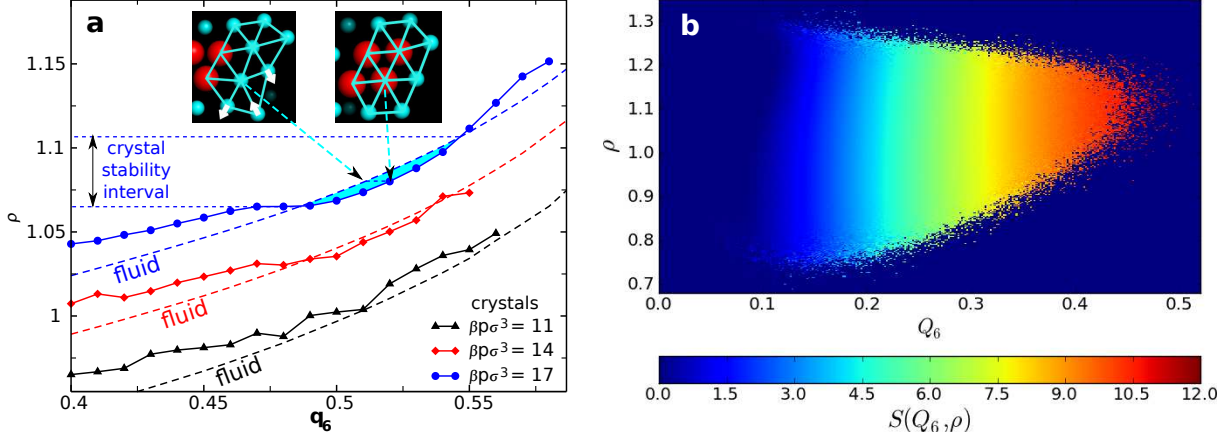


FIG. 2: **Roles of density and bond orientational order in crystal nucleation.** **a**, Relation between density (ρ) and bond orientational order (q_6) in the metastable liquid for different pressures, $\beta p \sigma^3 = 11, 14, 17$. Dashed lines are averages over particles in liquid-like environments, whereas full lines+symbols are averages over those in crystal-like environments. For each pressure, the stable phase is given by the lowest line. For $\beta p \sigma^3 = 11$, which is just below the melting pressure $\beta p \sigma^3 = 11.54$, the liquid line is always stable against the crystal line. But as the pressure is increased the crystal line crosses the liquid line to become the stable phase. The transition from liquid-like to crystal-like happens at constant density, and can be rationalized by the small cage rearrangements (as seen in the snapshots) which are sufficient to promote the transition with very little density change. At higher densities a second crossover occurs, and the liquid branch becomes stable again against the crystal-like branch. **b**, Probability density for the structural order parameter S in the (Q_6, ρ) plane. The number of connected neighbours grows continuously from 0 to 12 from the liquid to the crystal phase. Contour lines are almost parallel to the ρ axis signalling that crystallization is promoted mostly by bond orientational order. Regions of high ρ contain particles in a range of environments from liquid-like to crystal-like, which means that density fluctuations alone are not sufficient to promote crystallization.

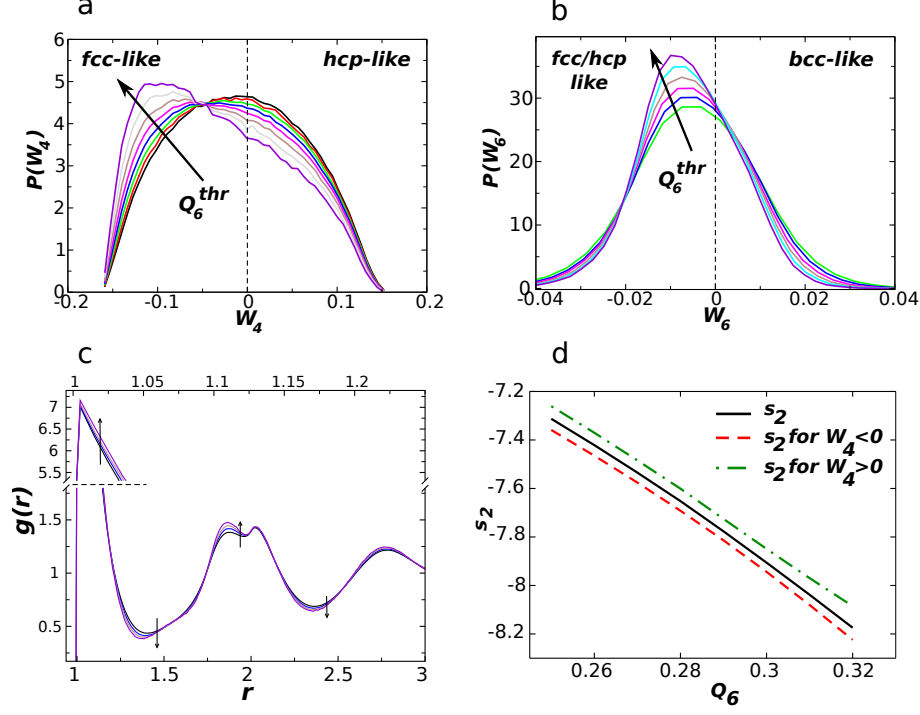


FIG. 3: Mechanism of polymorph selection. **a**, Order parameter W_4 for liquid particles having $Q_6 > 0.25, 0.26, 0.27, 0.28, 0.29, 0.30, 0.31, 0.32$ (the order is given by the arrow). The dashed line is the probability distribution for crystalline particles in the same system. As Q_6 increases, the regions of high structural order in the liquid are characterized by a growing population of fcc-like clusters. **b**, Order parameter W_6 for liquid particles having $Q_6 > 0.27, 0.28, 0.29, 0.30, 0.31, 0.32$. As Q_6 increases, the distributions move to lower and negative values of W_6 , thus showing no preference for the bcc symmetry ($W_6 > 0$). Ordering seen in the pair correlation function. **c**, Pair distribution function, $g(r)$, for liquid particles having $Q_6 > 0.25, 0.28, 0.30, 0.32$ (the order is given by the arrows). The y axis has been split to display the first maximum of $g(r)$ (the corresponding x scale is on the top axis). Regions of high Q_6 clearly show an enhanced shoulder in the second peak of the pair distribution function, which is a precursor to crystallization. **d**, Two-body excess entropy s_2 (continuous line), calculated for liquid particles with $Q_6 > Q_6^{\text{thr}}$; the dashed and dotted-dashed lines are instead calculated for liquid particles having $W_4 < 0$ and $W_4 > 0$ respectively. fcc-like particles ($W_4 < 0$) in regions of high Q_6 are thus favoured for crystallization over hcp-like particle ($W_4 > 0$).

Supplementary Information for “The microscopic pathway to crystallization in supercooled liquids”

John Russo and Hajime Tanaka

Institute of Industrial Science, University of Tokyo

4-6-1 Komaba, Meguro-ku, Tokyo 153-8505, Japan

Supplementary Information is organized as follows. First we discuss in more details the methods employed in our study, with emphasis on the crystal identification protocol. We then show that the microscopic mechanism of crystallization discussed for HS in the main text, also applies to other relevant classes of systems. In particular we examine: i) the Gaussian Core model (GCM), a model for self-avoiding polymers in an athermal solvent, which belongs to the class of ultrasoft potentials [1]; ii) the Mw model, a model for water, which belongs to the class of tetrahedrally coordinated liquids [2].

Crystal identification

The definitions of the order parameters employed in our study are reported in the *Methods* section. Fig. S4 shows the distribution of these order parameters for both the supercooled liquid and the bulk fcc, hcp and bcc crystals at reduced pressure $\beta p \sigma^3 = 17$.

The Q_4 - Q_6 map (Fig. S4a) shows that crystal structures are always located at higher Q_6 than the liquid state. But the map is not effective for distinguishing between the different polymorphs due to the large overlap between the bcc and the hcp structures. Another warning concerning the use of this map for crystal identification regards its pressure dependence. As we saw in the main text, crystal particles form at conditions very far from bulk values and in particular the density of formation of the smallest nuclei is much lower than the final bulk density. By computing the $Q_4 - Q_6$ map at different average densities for the bulk crystals one sees that these maps significantly shift to lower Q_6 as density is decreased. We thus conclude that $Q_4 - Q_6$ maps cannot be reliably used for crystal identification. Instead, to identify the crystal polymorphs we take advantage of the different symmetries that the crystals have on the W_6 and W_4 axis. The bcc structure is in fact characterized by a positive W_6 distribution (Fig. S4c) whereas hcp and fcc both have negative W_6 but differ respectively

for their positive and negative values of W_4 (Fig. S4d). We have checked that these symmetries are left unchanged if computing the maps at different average densities (or pressures). We finally adopt the following criteria for crystal classification: First crystal particles are identified as described in Methods and SI. Then, we identify i) bcc particles as all crystal particles with $W_6 > 0$; ii) hcp particles as all crystal particles with $W_6 < 0$ and $W_4 > 0$; iii) fcc particles as all crystal particles with $W_6 < 0$ and $W_4 < 0$.

Now we justify the claim made in the article that high q_6 particles correspond to icosahedra. To spot icosahedra we follow the definitions in Ref. [3], which we briefly summarize here. Icosahedra can be identified by thresholding the value of the following order parameter

$$w_6(i) = \sum_{m_1, m_2, m_3=0}^6 \begin{pmatrix} 6 & 6 & 6 \\ m_1 & m_2 & m_3 \end{pmatrix} q_{6m_1}(i) q_{6m_2}(i) q_{6m_3}(i)$$

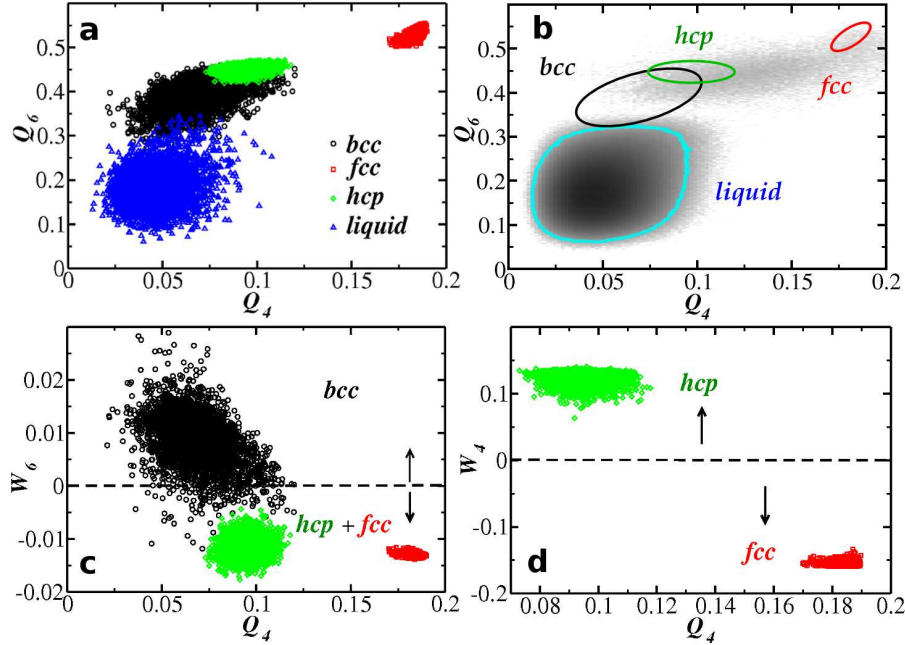


Fig. S4: **Order parameter maps for the thermal crystals and the supercooled state.** **a**, Q_4 - Q_6 plane. **c**, Q_4 - W_6 plane. **d**, Q_4 - W_4 plane. In **b** the probability distribution for the supercooled state is superimposed on the Q_4 - Q_6 map for the perfect crystals (fcc, hcp and bcc). The maps show that crystals have higher values of Q_6 than the supercooled liquid. We can also see that the supercooled liquid prior to crystal nucleation consists of its major liquid portion (the dark gray region; $Q_6 < 0.35$) and minor solid portion (the tint gray region; $Q_6 > 0.35$). The polymorphs can be identified by exploiting their symmetries along different axes: bcc crystals have $W_6 > 0$, whereas hcp and fcc crystals are both characterized by $W_6 < 0$ and have respectively $W_4 > 0$ and $W_4 < 0$.

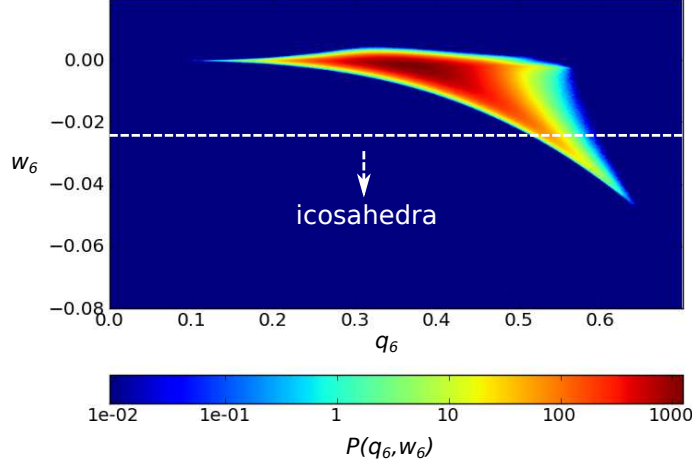


Fig. S5: **Probability density map in the q_6 – w_6 plane for the metastable fluid at $\beta p \sigma^3 = 17$.** The map clearly shows that high q_6 particles are characterized by a low value of w_6 , and are thus particles in icosahedral environment.

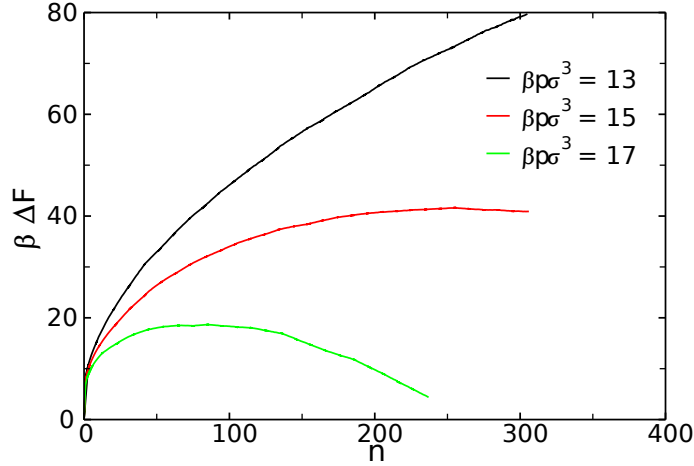


Fig. S6: **Free energy barrier for the system at $\beta p \sigma^3 = 13, 15, 17$, obtained from Umbrella Sampling simulations.**

where the term in parentheses is the Wigner $3-j$ symbol (which is different from zero only when $m_1 + m_2 + m_3 = 0$), and q_{lm} are the Steinhardt bond orientational order parameters defined in the Methods section. Following Ref. [3] icosahedral particles can be identified as particles having $w_6 > 0.023$. As shown in Fig. S5, particles with high q_6 all lay within the region which identifies icosahedral environments. We have thus shown that the high q_6 particles, which form the final liquid stable branch at high densities, are in fact icosahedral particles.

With the criteria for identifying crystal particles it is possible to obtain the free energy barrier and the critical cluster size from Umbrella Sampling simulations, where a biasing

potential is added to the system Hamiltonian to sample crystalline clusters of large sizes. The details of the implementation can be found in Ref. [4]. Fig. S6 plots the free energy barrier $\beta\Delta F$ as a function of cluster size. The free energy barrier between the metastable liquid phase and the crystal phase at $\beta p\sigma^3 = 17$ is $\beta\Delta F \simeq 18$, and the size of the critical nucleus is $\simeq 80$. These results are in good agreement with the ones in Ref. [5]. In this condition crystallization is a rare event, for which not only long trajectories can be obtained for the supercooled melt, but also enough nucleation events can be observed spontaneously.

The composition of nuclei obtained from the spontaneously nucleating trajectories were compared with the ones obtained in equilibrium from the Umbrella Sampling configurations for nuclei of size up to 250 particles. No difference in the average composition of the nuclei was found between the Umbrella Sampling configurations and the configurations obtained from the Monte Carlo trajectories. This proves that the small clusters are in quasi-equilibrium, due to the presence of a free energy barrier.

Nuclei composition was calculated also for pressures $\beta p\sigma^3 = 13, 15$ with Umbrella Sampling configurations and no sensible change in the polymorph composition was found with respect to the reported pressure $\beta p\sigma^3 = 17$.

Gaussian Core model

The Gaussian Core model (GCM) describes the effective potential between the centres of mass of polymers dispersed in a good solvent. It consists of pairwise sum of Gaussian components, first introduced by Stillinger [1]. The GCM belongs to the class of ultra-soft potentials, for which there is no divergence at contact. Unlike HS, soft particles can crystallize in open structures, such as the bcc crystal. We have recently published a detailed account on the nucleation pathway in the GCM [6], and thus we report here the results relevant for our new analysis. In the following we study the nucleation in the GCM for $P = 0.05$ and $T = 0.0052$, where the units of length and energy are given by the standard deviation and amplitude of the Gaussian potential (as usual in the literature [7]). According to the phase diagram calculated in Ref. [8], the chosen state point has the bcc as the stable bulk crystal. We follow the crystallization of 200 isobaric Monte Carlo trajectories starting from a metastable fluid phase. Crystal particles are identified with the following set of parameters (defined in the previous section), $N_c = 9$ and $q_{\text{thr}} = 0.6$, and the different

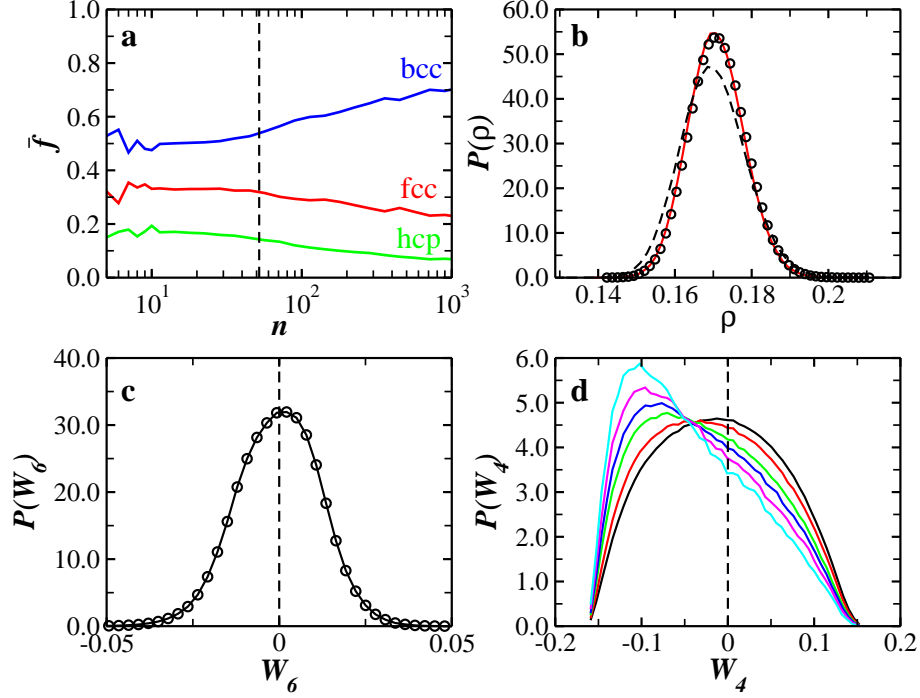


Fig. S7: **Polymorph selection in the GCM.** **a**, Fraction of particles (\bar{f}) in a given crystalline state as a function of the total crystal size n for $P = 0.01$. The vertical dashed line denotes the size of the critical nucleus n_c . **b**, Density probability distribution. The continuous and dashed line are the density histogram for solid and liquid particles respectively. The dots represent the density histogram for liquid particles fulfilling the condition $Q_6 > 0.3$. **c**, W_4 probability distribution for liquid particles having $W_6 < 0$ and Q_6 higher than a fixed threshold Q_6^{thr} . The threshold values plotted are $Q_6 > 0.25, 0.27, 0.29, 0.30, 0.31, 0.32$. **d**, W_6 probability distribution for liquid particles having $Q_6 > 0.3$.

polymorphs distinguished with the same criteria as HS.

Fig. S7a shows the composition of crystalline nuclei as a function of the nucleus size, for the hcp, fcc and bcc polymorphs. The bcc phase is the dominant phase and its fraction increases as the crystal nucleus gets bigger. Particles in the fcc phase account for $\sim 30\%$ of the solid particles in the small nuclei, and this fraction decreases as the nuclei become bigger. The hcp phase accounts only for $\sim 20\%$ of solid particles in small nuclei, with this fraction steadily decreasing as the nuclei become bigger. The vertical dashed line in Fig. S7a indicates the size of the critical nucleus (n_c) obtained from the mean-first passage time analysis (see Ref. [9]). The composition of the nucleus for $n < n_c$ is approximately constant, whereas, for $n > n_c$, the fraction of the bcc polymorph increases at the expenses of both the fcc and hcp phases.

Fig. S7b shows the density histogram for liquid (dashed line) and solid particles (con-

tinuous line). Circles in Fig. S7b display the density histogram for liquid particles having a value of Q_6 higher than 0.3, showing that it coincides with the density histogram of the solid particles. Also for the GCM, high Q_6 regions are characterized by the same density fluctuations as the crystalline particles.

From Fig. S7a we see that for $n < n_c$ half of the crystalline particles are in the bcc phase, whereas the other half are in the fcc or hcp phase. This is consistent with the W_6 map shown in Fig. S7c, which shows an almost symmetrical W_6 distribution of liquid particles having high Q_6 . So, unlike HS, the high Q_6 regions in the liquid phase have a symmetry which favours also the bcc phase, promoting its nucleation. Fig. S7a also shows a fraction of fcc particles twice the fraction of hcp particles. Again this is predicted from the W_4 probability distribution function in the liquid phase, depicted in Fig. S7d. As in HS, regions of high orientational order show a preference for the fcc symmetry.

Mw model for water

The monoatomic model of water (Mw) is essentially a reparametrization of the Stillinger-Weber potential to account for the structural and thermodynamic properties of water [2]. The model has been very successful in describing the supercooled behaviour of water and, unlike all-atom models, it crystallizes relatively easily. Because of its distinctive physical properties and its paramount importance, water is a very good test for our microscopic description of crystallization. Unlike both HS and GCM,

- the density of the solid phase is lower than the liquid phase. We should then expect an anticorrelation between bond orientational order and density, i.e. the density decreasing (instead of increasing, as in HS) with an increase of bond orientational order;
- the solid phases of water at ambient pressure are the hexagonal ice (Ih) and the cubic ice (Ic), providing a possibility to test our polymorph selection criteria for these target crystals.

To detect crystal particles we make use of the CHILL algorithm [10], which is a natural extension of the methods described previously for HS to account for the tetrahedral arrangement of particles. For particle i , we define the four closest neighbours ($j_1 \cdots j_4$) and for each

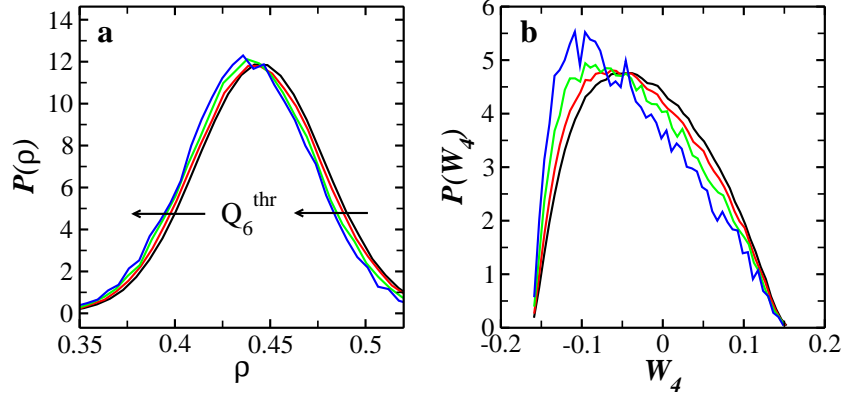


Fig. S8: **Polymorph selection in the Mw water.** **a**, Density probability distribution for liquid particles having $Q_6 > Q_6^{\text{thr}}$, with $Q_6^{\text{thr}} = 0.09, 0.10, 0.11, 0.12, 0.13$ and the order given by the arrow. **b**, W_4 probability distribution for the same set of particles as in panel **a**.

bond we compute the scalar product $s_3 = \hat{\mathbf{q}}_3(i) \cdot \hat{\mathbf{q}}_3(j)$. Staggered bonds are characterized by $s_3 < -0.8$ and eclipsed bonds by $-0.3 < s_3 < 0.1$. The Ih crystal is characterized by having one eclipsed bond and three staggered bond, whereas Ic crystal has all four bonds in a staggered configuration. Also defective crystal configurations are detected by following the rules in Ref. [10]. The definition of these defects varies somehow in the literature, as in Refs. [11, 12], but we tested that our results are independent of the details of this choice. Testing the symmetry of liquid particles is more subtle. In order to find an order parameter which can distinguish between the Ic and Ih symmetry, we need to take into account the second coordination shell, which comprises 16 molecules. In this case we have found that the W_4 provides a very good way to distinguish between Ih and Ic, with Ih having $W_4 > 0$ and Ic $W_4 < 0$.

Simulations at both $T = 180$ K [13, 14] and at $T = 220$ K [12] have shown that ice spontaneously nucleates preferentially in the Ic form. We run simulations at ambient pressure and at an intermediate temperature, $T = 206$ K, and confirm the preference for Ic nucleation over Ih nucleation. We then test the symmetry of regions of high bond orientational order in the liquid phase (not considering crystalline particles). Fig. S8a shows the density distribution for liquid particles of high bond orientational order, having $Q_6 > Q_6^{\text{thr}}$, confirming that indeed regions of high orientational order are anticorrelated with density. Fig. S8b finally shows the probability distribution on the W_4 axis for liquid particles with $Q_6 > Q_6^{\text{thr}}$. The distribution becomes more and more peaked towards negative values of W_4 , which correspond to the Ic symmetry, as bond orientational order increases in the liquid.

This explains why Ic crystals are the most abundant polymorph at this state point.

We have thus shown that in a large class of potentials (hard, ultrasoft and tetrahedral) nucleation occurs always in regions of high bond orientational order, and that these regions share the same symmetry of the nucleating solid phase. This suggests the universality of our scenario.

-
- [1] Stillinger, F. H. Phase transitions in the Gaussian core system. *J. Chem. Phys.* **65**, 3968–3974 (1976).
 - [2] Molinero, V. & Moore, E. B. Water modeled as an intermediate element between Carbon and Silicon. *J. Phys. Chem. B* **113**, 4008–4016 (2008).
 - [3] Leocmach, M. & Tanaka, H. Roles of icosahedral and crystal-like order in hard spheres glass transition submitted (2012).
 - [4] Auer, S. & Frenkel, D. Numerical simulation of crystal nucleation in colloids. *Adv. Polym. Sci.* **173**, 149–207 (2005).
 - [5] Fillion, L., Hermes, M., Ni, R. & Dijkstra, M. Crystal nucleation of hard spheres using molecular dynamics, umbrella sampling, and forward flux sampling: A comparison of simulation techniques. *J. Chem. Phys.* **133**, 244115 (2010).
 - [6] Russo, J. & Tanaka, H. Selection mechanism of polymorphs in the crystal nucleation of the Gaussian core model. *Soft Matter* **8**, 4206–4215 (2012).
 - [7] Likos, C. N. Effective interactions in soft condensed matter physics. *Phys. Rep.* **348**, 267–439 (2001).
 - [8] Prestipino, S., Saija, F. & Giaquinta, P. V. Phase diagram of the Gaussian-core model. *Phys. Rev. E* **71**, 050102 (2005).
 - [9] Wedekind, J., Strey, R. & Reguera, D. New method to analyze simulations of activated processes. *J. Chem. Phys.* **126**, 134103 (2007).
 - [10] Moore, E. B., de La Llave, E., Welke, K., Scherlis, D. & Molinero, V. Freezing, melting and structure of ice in a hydrophilic nanopore. *Phys. Chem. Chem. Phys.* **12**, 4124–4134 (2010).
 - [11] Romano, F., Sanz, E. & Sciortino, F. Crystallization of tetrahedral patchy particles in silico. *J. Chem. Phys.* **134**, 174502 (2011).
 - [12] Reinhardt, A. & Doye, J. P. K. Free energy landscapes for homogeneous nucleation of ice for

- a monatomic water model. *J. Chem. Phys.* **136**, 054501 (2012).
- [13] Moore, E. B. & Molinero, V. Ice crystallization in waters no-mans land. *J. Chem. Phys.* **132**, 244504 (2010).
- [14] Moore, E. & Molinero, V. Is it cubic? Ice crystallization from deeply supercooled water. *Phys. Chem. Chem. Phys.* **13**, 20008 (2011).